CELL CYCLE
2022, VOL. 21, NO. 20, 2145–2164
https://doi.org/10.1080/15384101.2022.2087280

Taylor & Francis
Taylor & Francis Group

RESEARCH PAPER

circFCHO2 promotes gastric cancer progression by activating the JAK1/STAT3 pathway via sponging miR-194-5p

Zhe Zhang[a], Chengying Sun[a], Yan Zheng[b], and Yanying Gong[b]

[a]Department of Geriatrics, the Fourth Affiliated Hospital of China Medical University, Shenyang, Liaoning, China; [b]Department of Gastroenterology, the Fourth Affiliated Hospital of China Medical University, Shenyang, Liaoning, China

ABSTRACT

circFCHO2 has been revealed to be overexpressed in gastric cancer (GC) patients. This article identified the function of circFCHO2 on GC progression. The expression of circFCHO2, miR-194-5p and JAK1 in 30 GC patients and cells was monitored by quantitative reverse transcription-polymerase chain reaction. circFCHO2 localization in GC cells was monitored by RNA fluorescence in situ hybridization. Cell counting kit-8 assay, 5-ethynyl-2-deoxyuridine staining, transwell experiment, tube formation and sphere formation experiments were applied to detect GC cell proliferation, invasion, angiogenesis and cancer stem cell characteristics. Dual-luciferase reporter gene assay, RNA pull down assay and RNA immunoprecipitation experiment were utilized to research the binding between two genes. In vivo tumorigenesis and lung metastasis were studied using nude mice. Immunohistochemistry and hematoxylin–eosin staining were conducted. Protein expression was assessed by Western blot. Serum exosomes of GC patients and healthy participants were isolated. circFCHO2 up-modulation in GC patients was related to poor outcome. circFCHO2 was located in the cytoplasm of GC cells. circFCHO2 silencing weakened the proliferation, invasion, angiogenesis and stem cell characteristics of GC cells. miR-194-5p knockdown counteracted this effect. circFCHO2 activated the JAK1/STAT3 pathway by sponging miR-194-5p. miR-194-5p overexpression attenuated the malignant phenotypes of GC cells. JAK1 overexpression abrogated this effect. circFCHO2 silencing weakened GC cells growth and lung metastasis in vivo. circFCHO2 was up-modulated in serum exosomes of GC patients. circFCHO2 was an oncogene in GC by activating the JAK1/STAT3 pathway via sponging miR-194-5p. circFCHO2 might be a novel target and diagnostic marker for GC.

ARTICLE HISTORY
Received 29 December 2021
Revised 18 May 2022
Accepted 30 May 2022

KEYWORDS
GC; circFCHO2; miR-194-5p; JAK1/STAT3; progression; metastasis

Introduction

Gastric cancer (GC) ranks the 5th among the common cancers in the world. It is the 3rd reason of cancer-related death [1]. The onset of GC includes multiple factors, such as Helicobacter pylori bacteria infection, genetic predisposition, tobacco smoking, alcohol drinking, unhealthy eating habits and dusty work environments [2]. GC is usually diagnosed at an advanced stage due to early symptoms that are not easily noticed. Therefore, the 5-year survival of GC is still no more than 30% although after the resection treatment and adjuvant treatment strategies such as chemotherapy [3]. The elucidation of the internal molecular mechanisms of the pathogenesis and malignant development of GC is conductive to the development of precise treatment.

Circular RNAs (circRNAs) are a class of endogenous transcripts, which are featured by covalently closed-loop structures. Different from linear RNA, circRNAs have the advantage of structural stability, and thus are difficult to be degraded by RNase R due to the lack of free terminal structures [4]. circRNAs are anticipated to be promising precise therapeutic targets for GC, because of its structural stability advantage [5]. The effect of several circRNAs in GC progression has been revealed. For instance, circTMEM87A not only exacerbates GC cells in vitro growth and invasion but also facilitates in vivo tumor growth and lung metastasis. High circTMEM87A expression in GC

CONTACT Yanying Gong 13840339116@163.com Department of Gastroenterology, the Fourth Affiliated Hospital of China Medical University, No. 102, Nanqi Road, Heping District, Shenyang, 110005, Liaoning, China.
Supplemental data for this article can be accessed online at https://doi.org/10.1080/15384101.2022.2087280

patients indicates an unfavorable clinical outcome [6]. circAFF2 silencing attenuates the proliferation, migration and invasion of GC cells, and delays GC cell growth in vivo [7]. Similarly, circ_0000039, circ_0081146 and circ_0110389 are identified as tumor-promoting circRNAs in GC [8–10]. Conversely, some circRNAs possess the opposite functions in GC, such as circITCH, circ_0072309, circ_0001017 and circRNA_0009172. These circRNAs are lowly expressed in GC patients, associating with poor clinical outcome. The up-regulation of these circRNAs attenuates the malignant phenotype of GC cells [11–14]. The elucidation of the exact function of these circRNAs provides novel directions for the target treatment of GC. Nevertheless, a large number of circRNAs functioning in GC progression is still largely unexplored.

circFCHO2 has been recently discovered to be an independent prognostic factor for better prognosis of cytogenetically normal acute myeloid leukemia patients, such as longer overall survival and disease-free survival [15]. However, the exact function of circFCHO2 in solid tumors has not been elucidated currently. At present, only one literature has revealed that circFCHO2 (circBase ID: hsa_circ_0072979) is aberrantly overexpressed in GC tissues than that in paracancer tissues of GC patients [16]. Unfortunately, the literature was failed to perform in-depth research to clarify the exact function of circFCHO2 in GC progression. Thus, this article was designed to explore the exact influence of circFCHO2 on the malignant development of GC.

In order to clarify the internal mechanism of circFCHO2 regulating GC progression, we discovered that miR-194-5p possessed mutual binding sites of circFCHO2 through Circinteractome. Thus, the present study speculated that circFCHO2 might modulate the progression of GC by targeting miR-194-5p. The Janus kinase-1 (JAK1)/signal transducer and activator of transcription 3 (STAT3) signaling pathway has been confirmed to be participated in the progression of multiple tumors, including GC [17–19]. In our preliminary study, we detected the up-modulated JAK1 expression in GC cells. Thus, we inferred that the JAK1/STAT3 pathway might be the down-stream pathway of miR-194-5p. Previous study has been revealed that JAK1 can be acted as a target of miRNAs [20,21]. Thus, we predicted by TargetScan online software whether JAK1 was a target of miR-194-5p. Interestingly, it was showed that miR-194-5p contained binding site of JAK1. Therefore, it was speculated that circFCHO2 might regulate the progression of GC via targeting miR-194-5p/JAK1. This article might provide important guidance for the target treatment of GC.

Methods

Patients and tissues

This study enrolled 30 GC patients from our hospital. None of them had cancer-related treatment history. All of them were identified as GC from March 2014 to November 2014 and treated by surgical resection. Among the 30 GC patients, 18 cases encountered lymph node metastasis. Tumor tissues and corresponding paired adjacent noncancerous tissues were collected and kept at −80°C in a refrigerator. Patients were followed up for 60 months after surgery.

This work had been approved by the ethics committee of the Fourth Affiliated Hospital of China Medical University in line with the Declaration of Helsinki (EC-2014-KS-01). The written informed consent had been voluntarily signed by all patients.

Isolation of human serum exosomes

Blood samples of 30 healthy participants and 30 GC patients were collected. Exosomes were separated using Total Exosome Isolation Kits (Bestbio, Shanghai, China) according to the manufacturer's directions. In short, blood samples were centrifuged for 20 min at 2000 × g and 4°C. The serum was then collected, followed by being mixed with exosome isolation reagent. After 2 min centrifugation at 15,000 × g, the supernatant was removed and exosomes at the centrifuge tube bottom were collected.

Transmission electron microscope (TEM) of exosomes

Exosomes were fixed in PBS containing 4% paraformaldehyde and 4% glutaraldehyde at 4°C. Then, the exosomes samples were dropped on a carbon-coated copper grid. Phosphotungstic acid solution (2%) was used to treat the carbon-coated copper grid for 30 s. The exosomes were observed under a TEM (JEM-1200EX, JEOL, Tokyo, Japan) at 80 kV acceleration voltage.

Cell culture

Normal human gastric epithelial cell line (GES-1) and GC cell lines (MKN28, HGC-27, MKN45 and AGS) were purchased from the Cell Bank of Chinese Academy of Sciences (Shanghai, China). Each cell line was individually maintained in Dulbecco's modified Eagle's medium (DMEM) containing 10% fetal bovine serum (FBS) at 37° C, 5% CO_2.

Actinomycin D and RNase R treatment

The structural stability of circFCHO2 was evaluated by Actinomycin D and RNase R treatment. HGC-27 and AGS cells were kept in DMEM containing 10% FBS and 2 mg/mL Actinomycin D (Solarbio, Beijing, China) for 6, 12, 18 and 24 h, respectively. At the specific time point, HGC-27 and AGS cells were collected to extract the total RNA by using TRIzol reagent (Boster, Wuhan, China). The level of linear FCHO2 and circFCHO2 was monitored by using quantitative reverse transcription-polymerase chain reaction (qRT-PCR).

Furthermore, HGC-27 and AGS cells were separately cultured by DMEM containing 10% FBS for 48 h. Then, the total RNA was extracted by TRIzol reagent treatment. RNase R (Beyotime, Shanghai, China) was used to treat the total RNA sample with a concentration of 3 U/μg. Total RNA sample without RNase R treatment was served as control. The level of linear FCHO2 and circFCHO2 was assessed by qRT-PCR.

RNA fluorescence in situ hybridization (FISH) experiment

HGC-27 and AGS cells were cultured in 6-well plates by DMEM containing 10% FBS at 37°C, 5% CO_2. Notably, a sterile coverslip was placed on the bottom of each well before inoculation. After 24 h, the coverslip was taken out and 4% paraformaldehyde was then dropped onto cells for 2 h fixation at 4°C. Triton X-100 (0.5%) was utilized to treat cells for 15 min. Cells were incubated by Alexa Fluor 488 labeled circFCHO2 probe (GeneChem, Shanghai, China) for 12 at 4°C. Nucleus staining was conducted by using 4,6-diamidino-2-phenylin-dole (DAPI). The staining time was 10 min. For clinical tissues of GC patients, the tissue sections with a thickness of 5 μm were prepared after tissues being embedded into paraffin. Then, the sections were dewaxed by xylene and rehydrated by gradient ethanol. Then, sections were experienced treatment as described above. At last, cells and tissues were placed under a fluorescence microscope (Nikon, Tokyo, Japan) for observation. The expression of circFCHO2 was presented as green fluorescence, while nucleus was stained with blue fluorescence.

Separation of nucleus and cytoplasm

Nuclear/Cytosol Fractionation Kit (AmyJet Scientific, Wuhan, China) was applied for the separation of cytoplasm and nucleus in accordance with the instructions. In brief, after being harvested, HGC-27 and AGS cells were washed by phosphate buffer saline (PBS) for 3 times. Then, cells were treated by ice-cold cell fractionation buffer for 10 min, followed by being centrifuged for 5 min at 500 × g, 4°C. Cytoplasm and nucleus (deposited on the bottom) were collected separately. circFCHO2 expression in the nucleus and cytoplasm was monitored by qRT-PCR.

Cell transfection

Lipofectamine 3000 (Thermo Fisher Scientific, Waltham, MA, USA) was applied for the transfection. circFCHO2 shRNA, shRNA negative control (NC), miR-194-5p inhibitor, inhibitor NC, miR-

194-5p mimics, mimics NC, JAK1 overexpression vector and empty vector were all commercially purchased from GeneChem (Shanghai, China). HGC-27 and AGS cells maintained in DMEM without FBS were transfected or co-transfected in line with the instructions of Lipofectamine 3000. After transfection, cells were cultured at 37°C, 5% CO_2 by DMEM containing 10% FBS for 48 h. The determination of transfection efficiency was assessed by using qRT-PCR or Western blot.

Cell counting kit-8 (CCK-8) assay

HGC-27 and AGS cells (1×10^4 cells) were cultured in 96-well plates in 100 μL of DMEM with 10% FBS. After cultured for specific time (0, 24, 48 and 72 h) at 37°C, 5% CO_2, CCK-8 reagent was added into each well with 10 μL per well. Thereafter, cells were incubated for 2 h at 37°C. The optical density (OD) value was monitored by a porous microplate reader (Bio-TekR Instruments, Inc., Winooski, Vermont, USA) at 450 nm wavelength.

The 5-ethynyl-2-deoxyuridine (EdU) staining

HGC-27 and AGS cells (1×10^5 cells) were separately seeded into 6-well plates and cultured for 48 h with 1 mL of DMEM containing 10% FBS. After removing the remaining liquid, cells were fixed by 4% paraformaldehyde for 10 min. Then, Triton X-100 solution (Beyotime, Shanghai, China) was added into each well to treat cells for 30 min. According to the instruction, EdU assay kit (ab219801, Abcam, Shanghai, China) was employed to detect the proliferation.

Transwell experiment

HGC-27 and AGS cells (1×10^5 cells) dispersed in 500 μL of DMEM (serum free) were inoculated into transwell inserts pre-coating with Matrigel. The Transwell inserts were inserted into 6-well plates. For the lower chamber, a total of 600 μL of DMEM containing 10% FBS was filled. After 24 h incubation at 37°C, 5% CO_2, the invasion cells were treated by 4% paraformaldehyde for fixation. Cell staining was implemented by using 0.1% crystal violet. The number of invasion cells was observed and counted under a microscope in 5 random fields of view.

Tube formation experiment

The tube formation assay of GC cells was carried out according to a previous study [22]. Briefly, Matrigel was coated into 96-well plates with 100 μL per well. The plates were placed for 30 min at 37 C. After that, HGC-27 and AGS cells (4×10^4 cells) were inoculated into the above 96-well plates for 48 h culture with 100 μL of DMEM containing 10% FBS. Then, cells were observed and photographed under a microscope. The tube length was measured.

Sphere formation experiment

HGC-27 and AGS cells were harvested, followed by being suspended into DMEM with 10% FBS. The density of cells was 1×10^4 cells/mL. Low attachment dishes were used for sphere formation assay. Briefly, a total of 1 mL of the cell suspension was inoculated into the low attachment dishes. Cells were cultured for 3 weeks at 37°C, 5% CO_2. During this process, fresh DMEM containing 10% FBS was changed every 3 days. The number of sphere formation was counted under a microscope.

RNA pull down assay

circFCHO2 probe and Oligo probe were commercially provided from GeneChem (Shanghai, China). HGC-27 and AGS cells cultured for 48 h were collected and then incubated by RNA lysis buffer. The lysate was incubated with circFCHO2 probe and Oligo probe for 4 h. Then, the circFCHO2-miRNAs complexes were captured by Dynabeads M-280 Streptavidin (Dynal, Oslo, Norway) overnight. The operation was finished strictly based on the instructions. The bound RNAs were subjected to purification via using Trizol reagent (Boster, Wuhan, China). The enrichment of miR-194-5p, miR-151a-3p and miR-526-5p was qualified by qRT-PCR.

Dual luciferase reporter gene assay

Through bioinformatics analysis of three online forecasting sites (Starbase, CircBank and Circinteractome), miR-194-5p was discovered to possess mutual binding sites of circFCHO2 and JAK1. The circFCHO2 and JAK1 fragments of wild-type (Wt) and mutant-type (Mut) sequences were designed, amplified and cloned onto the pmirGLO luciferase reporter vectors (Promega, Madison, WI, USA) based on the instructions. HGC-27 and AGS cells seeded in DMEM (serum free) were co-transfected by miR-194-5p mimics and pmirGLO vectors, or by mimics NC and pmirGLO vectors in line with Lipofectamine 3000 instructions. Then, cells were culture for 48 h. The luciferase activity was monitored by using the Dual-Luciferase Reporter Assay System (Promega, Madison, WI, USA) in line with the instructions. The determination of the relative luciferase activity was normalized to Renilla luciferase activity.

RNA immunoprecipitation (RIP) experiment

The binding relationship between circFCHO2 and miR-194-5p was verified by RIP experiment via utilizing a Magna RIP kit (Millipore, Bedford, MA, USA). The operation was executed strictly based on the instructions. In brief, HGC-27 and AGS cells were incubated by RNA lysis buffer. The lysate was obtained, followed by treating with RIP immunoprecipitation buffer. The RIP immunoprecipitation buffer contained protein A/G sepharose beads conjugated with Ago-2 antibody (1:100, ab5072, Abcam, Shanghai, China) or IgG antibody (1:100, ab2410, Abcam, Shanghai, China). RNeasy Mini Kit (Qiagen, Hilden, Germany) was utilized for the extraction of the immunoprecipitated RNA. The enrichment of circFCHO2 and miR-194-5p was determined by qRT-PCR.

In vivo tumorigenesis and lung metastasis

Animal experiments had been approved by the animal ethics committee of Laboratory Animal Resources, Chinese Academy of Sciences (AR2021010847).

BALB/c nude mice (4 weeks old, n = 24) were commercially obtained from the Shanghai Laboratory Animals Center of the Chinese Academy of Sciences (Shanghai, China). Mice were housed in a 12 h day and night cycle room at 22°C. Food and water were given access freely.

AGS cells stably transfected by circFCHO2 shRNA and NC were dispersed into PBS. The concentration of cells was 1×10^7 cell/100 μL. Then, three mice were randomly selected for subcutaneous injection of the circFCHO2 shRNA-transfected AGS cells. Another three mice were subcutaneously injected from the shRNA NC-transfected AGS cells. The injection site was on the right side of the back, and 100 μL of the cell suspension was injected per mice. After injection, the tumor size was calculated every 7 days by (long diameter × short diameter ^{2})/2. All mice were euthanized after 28 days of injection. The subcutaneous xenograft tumor was stripped, weighted and kept at −80°C in a refrigerator.

For in vivo lung metastasis, circFCHO2 shRNA or shRNA NC transfected AGS cells (1×10^7 cell/100 μL PBS) were separately injected into three mice through tail vein. After 6 weeks, all mice were euthanized to collect the whole lungs. The lung tissues of mice were maintained at −80°C in a refrigerator. Additionally, for lymphatic metastasis, six mice were injected with circFCHO2 shRNA transfected AGS cells (1×10^7 cell/100 μL PBS), and the other six mice were injected with shRNA NC transfected AGS cells (1×10^7 cell/100 μL PBS) through tail vein. Mice were euthanized after 6 weeks to detect the lymphatic metastasis.

Immunohistochemistry (IHC) and hematoxylin-eosin (HE) staining

Ki67 expression in the subcutaneous xenograft tumor from mice was assessed by IHC. Xenograft tumor was cut into sections to a thickness of 5 μm. These sections were immersed into xylene, gradient ethanol and deionized water for dewaxing and rehydration. After 10 min incubation with 3% H_2O_2 solution, the sections were boiled in citrate buffer (0.01 M, pH = 6.0) for 10 min for the antigen retrieval. Then, 10 min blocking of these sections was carried out by immersing the sections into 5% goat serum. Rabbit anti-Ki67 primary

antibody (1:100, ab15580, Abcam, Shanghai, China) was applied to probe the sections overnight at 4°C. Subsequently, the sections were treated with biotin-labeled secondary antibody (1:200, ab6720, Abcam, Shanghai, China) for 30 min at 37°C. Afterward, horseradish peroxidase-labeled streptavidin working solution (Beyotime, Shanghai, China) was utilized for 30 min incubation of the sections at 37°C. Then, diaminobenzidine (DAB) staining and hematoxylin counterstaining were conducted on the sections. The sections were experienced gradient alcohol dehydration and xylene transparency, followed by being sealed in neutral resin. The images of the sections were captured by applying a microscope (Nikon, Tokyo, Japan).

For HE staining, lung tissues of mice were sequentially experienced sliced, deparaffinized, and rehydrated as described above. The sections of the lung tissues were immersed into hematoxylin solution for 5 min staining. Then, the sections were stained by eosin solution for 2 min. Xylene transparency and gradient alcohol dehydration were performed on the sections sequentially. The sections were sealed in neutral resin and observed under a microscope (Nikon, Tokyo, Japan).

qRT-PCR

The extraction of total RNA in tissues, cells and exosomes was executed via using TRIzol reagent (Beyotime, Shanghai, China) in line with the manual. Nanodrop 2000 spectrophotometer (Thermo Fisher Scientific, Waltham, MA, USA) was used for the detection of the total RNA concentration. The synthesis of cDNA was implemented by using the PrimeScript RT Reagent Kit (Takara, Shiga, Japan) and miRNA First-Strand cDNA Synthesis Kit (Thermo Fisher Scientific, Waltham, MA, USA). The operation was finished strictly in accordance with the kit instructions. TB Green Premix Ex Taq (Takara, Shiga, Japan) was used for qPCR with the conditions as below: 10 min at 95°C, with 40 cycles of 30 s at 95°C, 30 s at 55°C and 30 s at 72°C. The primers were designed and synthesized by GeneChem (Shanghai, China), as follows: circFCHO2 (F: 5'-TCACCAGCAATCCAACTCC-3' and R: 5'-AGGTATCCTGATTTCCAAGGC-3'), FCHO2 (F: 5'-GGATGGAGGAGTAACGAACA-3' and R: 5'-CGCTGAGGAATTGTACTGC-3'), JAK1 (F: 5'-AAGACCGAGCAGGATGG-3' and R: 5'-TGATGTCCTTGGGCAGTT-3'), miR-194-5p (F: 5'-GGGTGTAACAGCAACTCCA-3' and R: 5'-TCCTCCTCTCCTTCCTTCTC-3'), miR-151a-3p (F: 5'-GGGCTAGACTGAAGCTCC-3' and R: 5'-GTTGTGGTTGGTTGGTTTGT-3'), miR-526b-5p (F: 5'-GCTCTTGAGGGAAGCACT-3' and R: 5'-GTTGTTGGTTGGTTGGTTGT-3'), GAPDH (F: 5'-ACGGATTTGGTCGTATTGGG-3' and R: 5'-TGATTTTGGAGGGATCTCGC-3'), U6 (F: 5'-GCTTCGGCAGCACATATACTAAAAT-3' and R: 5'-CGCTTCACGAATTTGCGTGTCAT-3'). U6 was considered as the internal control for the expression of miR-194-5p, miR-151a-3p and miR-526b-5p. GAPDH was regarded as the internal control for the expression of circFCHO2, FCHO2, JAK1 and STAT3. The $2^{-\Delta\Delta Ct}$ method was applied for the determination of relative expression of these genes. Additionally, to confirm the ring structure of circFCHO2, divergent primer and convergent primer of circFCHO2 were synthesized by GeneChem (Shanghai, China). The qRT-PCR products were researched by electrophoresis on 2% agarose gels.

Western blot

Protein extraction kit (Biochain Institute Inc., Hayward, CA, USA) was applied to isolate total proteins in tissues, cells and exosomes based on the instructions. BCA kit (Beyotime, Shanghai, China) was used to investigate the concentration of the total proteins. The separation of the total proteins was finished by using 10% sodium dodecyl sulfate-polyacrylamide gel electrophoresis (SDS-PAGE). The proteins were transferred onto polyvinylidene difluoride (PVDF) membranes (Millipore, Billerica, MA, USA) by electrotransfer. After blocking by 5% skimmed milk, the following primary antibodies were utilized to probe proteins overnight at 4°C: rabbit anti-JAK1 (1:1000, ab47435), rabbit anti-STAT3 (1:1000, ab226942), rabbit anti-p-STAT3 (1:1000, ab86430), rabbit anti-CD63 (1:1000, ab68418), rabbit anti-TSG101 (1:1000, ab228013), rabbit anti-ALIX (1:1000, ab76608) and rabbit anti-β-actin (1:1000, ab8227). The primary antibodies were purchased from Abcam (Shanghai, China). Horseradish peroxidase labeled goat anti-rabbit secondary

antibody (1:2000, ab6721, Abcam, Shanghai, China) was then dropped to probe the proteins for 2 h at room temperature. Enhanced chemiluminescence reagent (Pierce, Rockford, IL, USA) was added to the PVDF membranes in order to develop the protein blots. The gray value of the protein blots was qualified by the Image J software (National Institutes of Health, Bethesda, MD, USA). β-actin was as the internal control. Data from three independent replicate experiments were taken for statistical analysis.

Statistical analysis

All experiments were repeated three times independently. SPSS 19.0 software was applied for the statistical analysis data (mean ± standard deviation). Data comparison was implemented by using two tailed paired Student's t-test (for two groups) or one-way analysis of variance (ANOVA) followed by Tukey's post hoc test (for at least three groups). The 60-month survival and metastasis-free survival of GC patients were evaluated by Kaplan–Meier curve. The receiver operating characteristic (ROC) curve was made to evaluate whether the serum circ_0008797 level could be used as a potential indicator to diagnose GC. $P < 0.05$ meant a statistically significant difference.

Results

circFCHO2 expression was elevated in GC, associating with poor outcome

The information of circFCHO2 in human genome was shown in Figure S1 A. The expression of circFCHO2 in 30 pairs of tumor tissues and

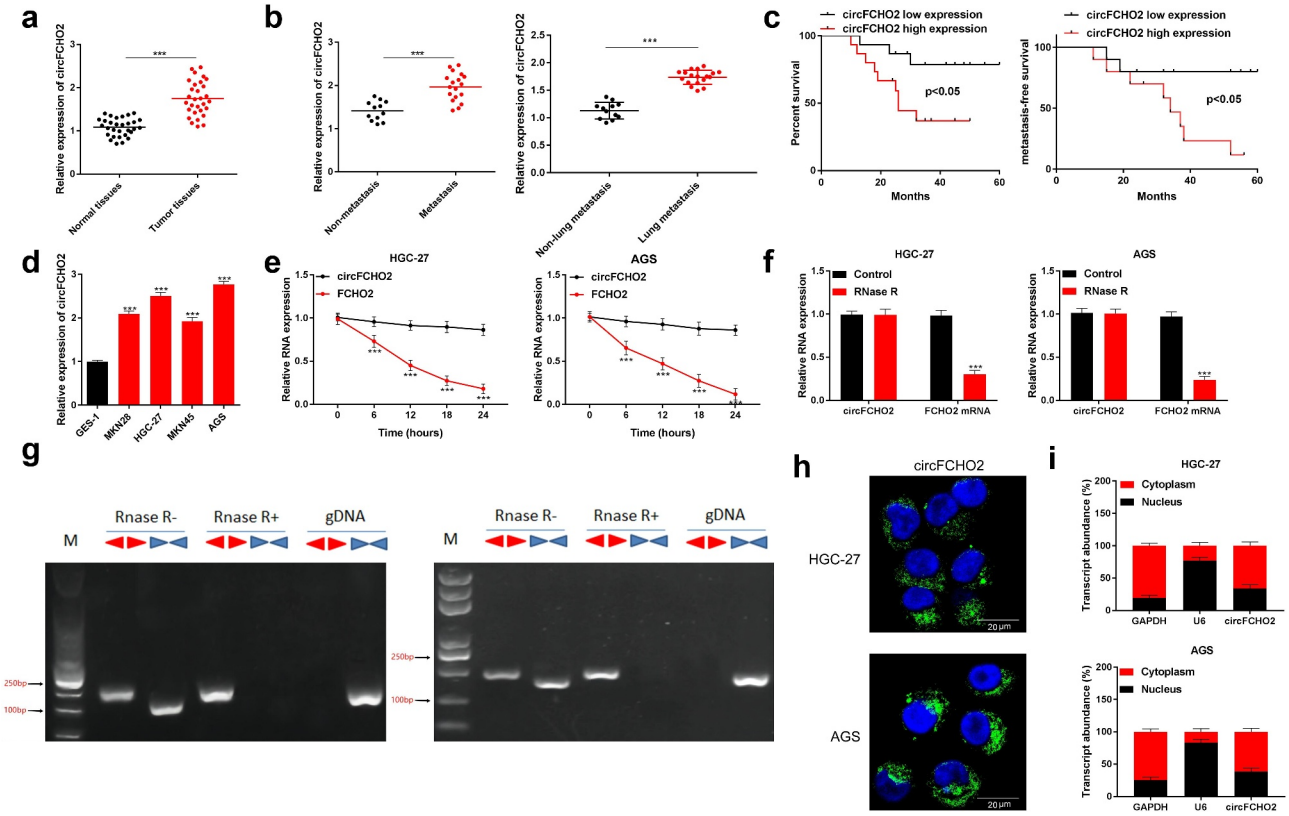

Figure 1. circFCHO2 expression was elevated in GC, associating with poor outcome.

(A) The expression of circFCHO2 in 30 pairs of tumor tissues and normal tissues adjacent to tumors was assessed using qRT-PCR. (B) The relationship between circFCHO2 and lymph node metastasis (and lung metastasis) of GC patients was researched via using qRT-PCR. (C) Kaplan–Meier curve was made to detect the 60-month survival and metastasis-free survival of GC patients. (D) circFCHO2 expression in cell lines was evaluated by qRT-PCR. (E) Actinomycin D treatment of GC cells was performed to detect the stability of circFCHO2 structure. (F) RNase R was applied for circFCHO2 structure stability detection. (G) The structure of circFCHO2 was monitored by the agarose gel analysis of the PCR production. (H) RNAFISH experiment was used to research the expression and location of circFCHO2 in GC cells. (I) Nuclear and cytoplasmic separation and qRT-PCR were used to detect the expression of circFCHO2 in the cytoplasm and nucleus of GC cells. *** $P < 0.001$.

normal tissues adjacent to tumors was assessed using qRT-PCR. As a result, the expression of circFCHO2 was distinctly increased in tumor tissues when compared with normal tissues ($P < 0.001$) (Figure 1(a)). Patients with lymph node metastasis (n = 18) showed much higher circFCHO2 expression in tumor tissues than those without lymph node metastasis (n = 12) ($P < 0.001$). At the same time, patients with lung metastasis exhibited higher circFCHO2 expression in tumor tissues than those without lung metastasis ($P < 0.001$) (Figure 1(b)). High circFCHO2 expression was monitored to be associated with poor 60-month survival of GC patients ($P < 0.05$). Simultaneously, GC cases with high circFCHO2 expression had lower metastasis-free survival than those with low circFCHO2 expression ($P < 0.05$) (Figure 1(c)). Therefore, high circFCHO2 expression indicated a poor prognosis of GC patients.

The expression of circFCHO2 in GC cells was researched. As a result, significantly increased circFCHO2 level was found in GC cell lines (MKN28, HGC-27, MKN45 and AGS) when compared with normal human gastric epithelial cell line (GES-1) ($P < 0.001$) (Figure 1(d)). Compared with FCHO2 mRNA, Actinomycin D and RNase R treatment obviously reduced the level of circFCHO2 ($P < 0.001$) (Figure 1(e,f)). Moreover, the structure of circFCHO2 was monitored by the agarose gel analysis of the PCR production. It could be noticed that circFCHO2 could be expressed in HGC-27 and AGS cells regardless of the presence or absence of RNase R (Figure 1(g)). Thus, circFCHO2 was stable in structure, which was hardly degraded by Actinomycin D and RNase R.

RNA FISH experiment showed that circFCHO2 was mainly expressed in the cytoplasm of HGC-27 and AGS cells (Figure 1(h)). Meanwhile, RNA FISH experiment of clinical tissues of GC patients exhibited that, circFCHO2 was highly expressed in the tumor tissues than that in adjacent normal tissues, and circFCHO2 was mainly expressed in the cytoplasm in the clinical tissues (Figure S1 B). qRT-PCR revealed that circFCHO2 was highly expressed in the cytoplasm of HGC-27 and AGS cells than that in the nucleus (Figure 1(i)). Thus, circFCHO2 was mainly located in the cytoplasm of GC cells.

circFCHO2 silencing weakened the proliferation, invasion, angiogenesis and stem cell characteristics of GC cells

HGC-27 and AGS cells of sh-circFCHO2 #1, #2, and #3 groups expressed significantly lower circFCHO2 than that of sh-NC group ($P < 0.001$) (Figure 2(a)), illustrating a successful transfection of HGC-27 and AGS cells. HGC-27 and AGS cells of sh-circFCHO2 #1 group had higher circFCHO2 silencing efficiency, which was used as the objects in the following studies (reset as sh-circFCHO2 group). The expression of FCHO2 mRNA was determined by qRT-PCR. Intriguingly, circFCHO2 silencing had no obvious effect on the expression of FCHO2 mRNA (Figure 2(b)).

Functional experiments were performed, including CCK-8 assay, EDU staining, transwell experiment, tube formation experiment and spheroidization experiment. As a result, matched with sh-NC group, HGC-27 and AGS cells of sh-circFCHO2 group presented prominently lower OD value, EDU positive staining, invasion number, tube length and spheroidization number ($P < 0.01$ or $P < 0.001$) (Figure 2(c,d,e,f and g)). These data indicated that circFCHO2 silencing weakened the proliferation, invasion, angiogenesis and stem cell characteristics of GC cells.

circFCHO2 exerted as a sponge of miR-194-5p

According to bioinformatics analysis of Circinteractome, miR-194-5p, miR-151a-3p and miR-526b-5p were predicted to be the potential targets of circFCHO2 (Figure 3(a)). Relative to Oligo probe, circFCHO2 probe enriched a large amount of miR-194-5p in HGC-27 and AGS cells ($P < 0.001$). However, miR-151a-3p and miR-526b-5p could not be obviously enriched by circFCHO2 probe when compared with Control probe (Figure 3(b)). Thus, miR-194-5p was selected as the target of circFCHO2.

The expression of miR-194-5p in 30 GC patients was investigated by using qRT-PCR. Significantly reduced miR-194-5p level was

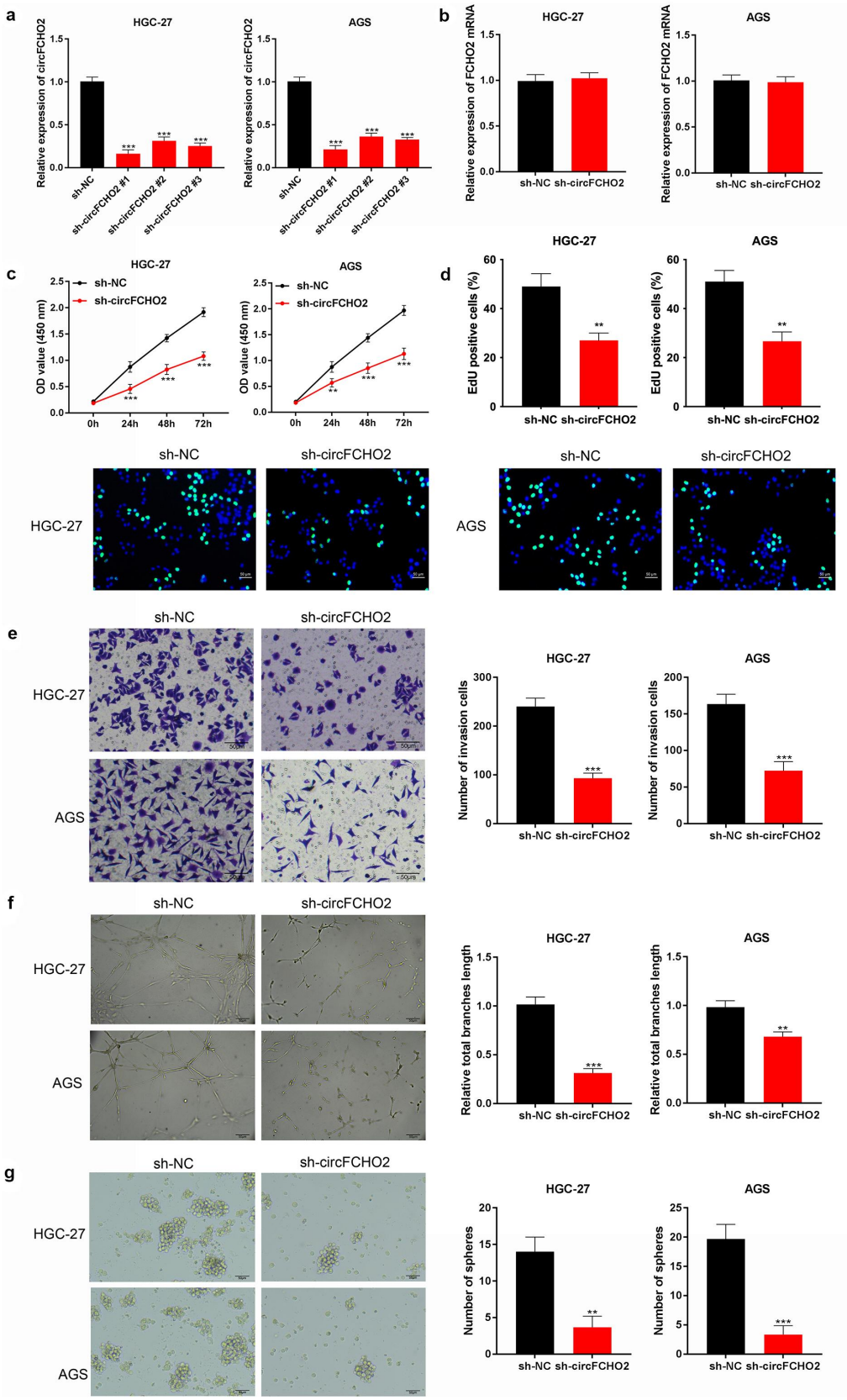

Figure 2. circFCHO2 silencing weakened the proliferation, invasion, angiogenesis and stem cell characteristics of GC cells.

(A) The transfection efficiency of cells was determined by qRT-PCR. (B) The expression of FCHO2 mRNA in GC cells was determined by qRT-PCR. (C) CCK-8 assay was applied to assay the proliferation ability of GC cells. (D) EDU staining was used to assess the proliferation ability of GC cells. (E) Transwell experiment was conducted to explore the invasion ability of GC cells. (F) Tube formation experiment was carried out to analyze the angiogenesis ability of GC cells. (G) Spheroidization experiment was used to research the stem cell characteristic detection of GC cells. ** $P < 0.01$ or *** $P < 0.001$.

observed in tumor tissues compared to adjacent normal tissues ($P < 0.001$) (Figure 3(c)). In GC tissues, a negative correlation was revealed between miR-194-5p and circFCHO2 expression ($P < 0.0001$) (Figure 3(d)). Moreover, much lower miR-194-5p expression was occurred in HGC-27 and AGS cell lines when matched with GES-1 cell line ($P < 0.001$) (Figure 3(e)).

The binding site of circFCHO2 and miR-194-5p was presented in Figure 3(f). Dual-luciferase reporter gene assay revealed that miR-194-5p mimic dramatically reduced circFCHO2-WT reporter luciferase activity in HGC-27 and AGS cells ($P < 0.001$). The circFCHO2-MUT reporter luciferase activity was not obviously changed by miR-194-5p mimic (Figure 3(g)). RIP assay indicated that circFCHO2 and miR-194-5p were both obviously enriched by anti-Ago2 than by anti-IgG ($P < 0.001$) (Figure 3(h)). In comparison to sh-NC group, markedly elevated miR-194-5p expression was found in HGC-27 and AGS cells of sh-circFCHO2 ($P < 0.001$) (Figure 3(i)). Hence, all of these data illustrated that circFCHO2 was a sponge of miR-194-5p. The expression of miR-194-5p could be directly suppressed by circFCHO2.

miR-194-5p knockdown partially reversed the inhibition of circFCHO2 silencing on the malignant phenotype of GC cells

miR-194-5p inhibitor as well as inhibitor NC were separately used to transfect HGC-27 and AGS cells. qRT-PCR showed that HGC-27 and AGS cells of miR-194-5p inhibitor group had much lower miR-194-5p expression than that of NC inhibitor group ($P < 0.001$) (Figure 4(a)). Thus, miR-194-5p inhibitor and inhibitor NC were successfully transfected into HGC-27 and AGS cells.

After transfection, cell proliferation, invasion, angiogenesis and stem cell characteristics were explored through CCK-8 assay, EDU staining, transwell experiment, tube formation experiment and spheroidization experiment. As a result, relative to HGC-27 and AGS cells in sh-NC group, distinctly reduced OD value, EDU positive staining cells, invasion number, tube length and spheroidization number were found in sh-circFCHO2 group ($P < 0.01$ or $P < 0.001$). Intriguingly, matched to sh-circFCHO2 group, HGC-27 and AGS cells of sh-circFCHO2 + miR-194-5p inhibitor presented obviously elevated OD value, EDU positive staining cells, invasion number, tube length and spheroidization number ($P < 0.05$ or $P < 0.01$ or $P < 0.001$) (Figure 4(b-e and f)).

circFCHO2 promoted the activity of the JAK1/STAT3 pathway by sponging miR-194-5p

JAK1 contained mutual binding site of circFCHO2 (Figure 5(a)). Dual-luciferase reporter gene assay illustrated that miR-194-5p mimic can directly reduce the luciferase activity of JAK1-WT reporter in HGC-27 and AGS cells ($P < 0.001$). However, JAK1-MUT reporter luciferase activity could not be obviously affected by miR-194-5p mimic (Figure 5(b)). In the 30 GC patients, JAK1 was remarkably overexpressed in tumor tissues relative to adjacent normal tissues ($P < 0.001$) (Figure 5(c)). The JAK1 mRNA level was negatively correlated with miR-194-5p ($P = 0.0079$) and positively correlated with circFCHO2 ($P = 0.0006$) in tumor tissues of GC patients (Figure 5(d -e)).

Additionally, HGC-27 and AGS cells exhibited much higher JAK1 protein expression than GES-1 cell line ($P < 0.001$) (Figure 5(f)). miR-194-5p mimic distinctly reduced JAK1 protein expression in HGC-27 and AGS cells ($P < 0.001$) (Figure 5(g and h)). In contrast to sh-NC, HGC-27 and AGS cells of sh-circFCHO2 group expressed less JAK1 and p-STAT3/STAT3 proteins ($P < 0.001$). Matched with sh-circFCHO2 group, the expression of JAK1 and p-STAT3/STAT3 proteins was obviously higher in HGC-27 and AGS cells of sh-circFCHO2 + miR-194-5p inhibitor group ($P < 0.01$ or $P < 0.001$) (Figure 5(i)).

JAK1 overexpression partially reversed the inhibition of miR-194-5p on the malignant phenotype of GC cells

As presented in Figure 6(a), the expression of JAK1 protein in HGC-27 and AGS cells was successfully elevated by JAK1 vector transfection ($P < 0.001$). Matched with miR-NC group,

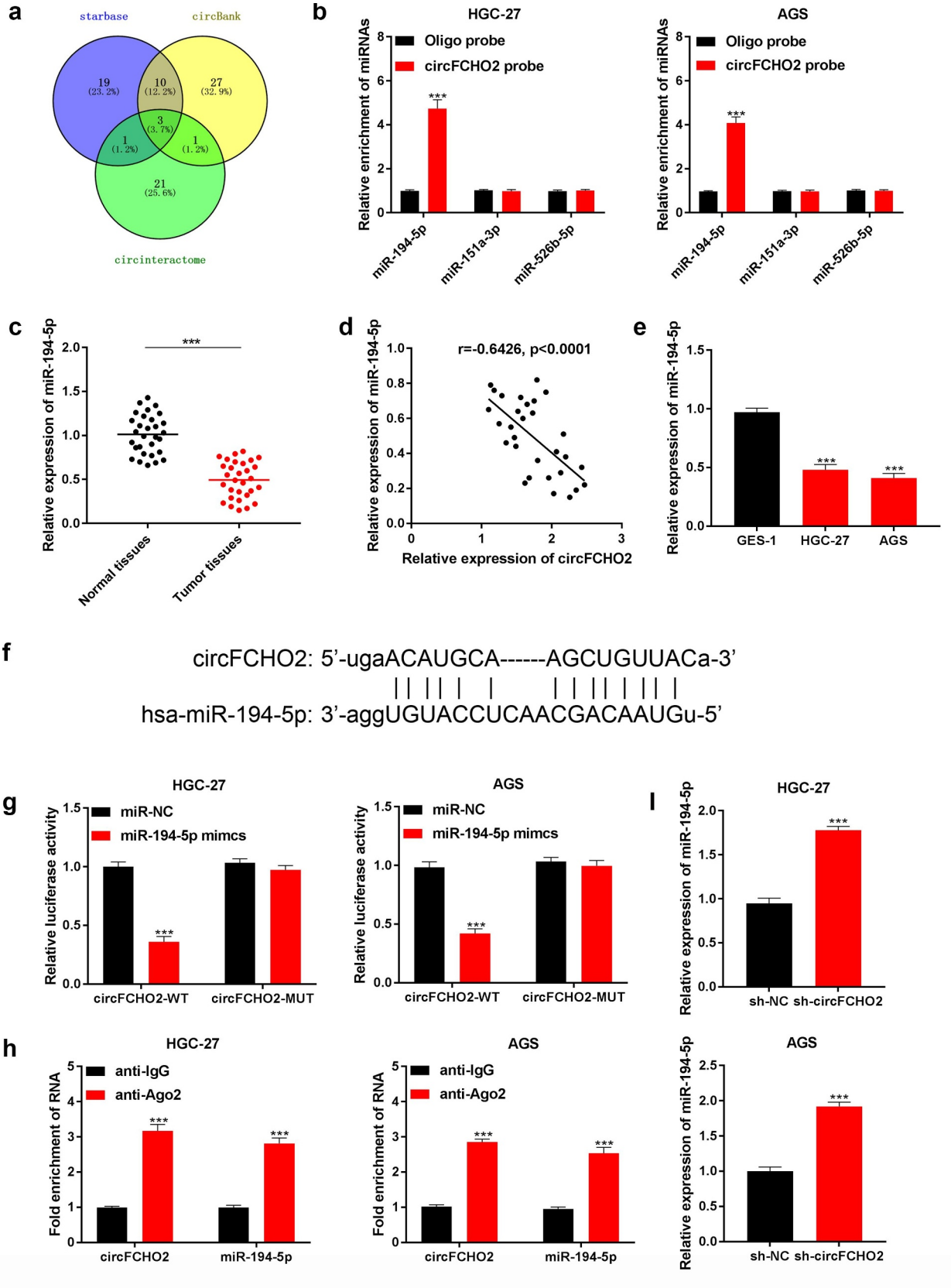

Figure 3. circFCHO2 exerted as a sponge of miR-194-5p.

(A) miR-194-5p, miR-151a-3p and miR-526b-5p were predicted as potential targets of circFCHO2. (B) RNA pull-down was applied to detect the binding relationship between circFCHO2 and the three mRNAs (miR-194-5p, miR-151a-3p and miR-526b-5p). (C) The expression of miR-194-5p in GC patients was investigated using qRT-PCR. (D) Pearson's correlation analysis researched the

HGC-27 and AGS cells of miR-194-5p group had prominently lower OD value, EDU positive staining cells, invasion number, tube length and spheroidization number ($P < 0.001$). Oppositely, relative to HGC-27 and AGS cells of miR-194-5p group, significantly higher OD value, EDU positive staining cells, invasion number, tube length and spheroidization number were observed in miR-194-5p + JAK1 group ($P < 0.05$ or $P < 0.01$ or $P < 0.001$) (Figure 6(b-e and f)).

circFCHO2 silencing weakened the in vivo growth and lung metastasis of GC

In vivo experiment was implemented by recruiting nude mice. Mice of sh-circFCHO2 group displayed much lower xenograft tumor volume and tumor weight than that of sh-NC group ($P < 0.001$) (Figure 7(a-b)). Moreover, mice of sh-circFCHO2 group expressed less Ki67 protein in xenograft tumor than that of sh-NC group (Figure 7(c)). qRT-PCR exhibited that, in comparison to xenograft tumor of sh-NC group, distinctly lower circFCHO2, higher miR-194-5p and lower JAK1 mRNA expression was found in sh-circFCHO2 group ($P < 0.001$) (Figure 7(d)). Western blot exhibited a significant decrease in JAK1 and p-STAT3/STAT3 protein expression in xenograft tumor of sh-circFCHO2 group when relative to sh-NC group ($P < 0.001$) (Figure 7(e)). Matched with sh-NC group, less lung nodules were found in the lung tissues of mice in sh-circFCHO2 group (Figure 7(f)). The original images of lung nodules are shown in Figure 7(g). Moreover, the effect of circFCHO2 on the lymphatic metastasis in vivo was researched. As a result, sh-circFCHO2 group showed less mice with lymphatic metastasis (n = 1) and more mice without lymphatic metastasis (n = 5) than sh-NC group (four mice with lymphatic metastasis and two mice without lymphatic metastasis, respectively) ($P < 0.01$) (Figure 7(h)).

circFCHO2 level in the serum exosomes was a sensitive and effective biomarker for the diagnosis of GC

The serum exosomes were isolated from GC patients and healthy participants. The exosomes were observed by TEM. From Figure 8(a), the diameter of serum exosomes was no more than 200 nm. The expression of exosomes markers was detected by Western blot, including CD63, TSG101 and ALIX. It was revealed that exosomes were successfully isolated (Figure 8(b)). The expression of circFCHO2 was distinctly higher in the serum exosomes of GC patients compared to healthy participants ($P < 0.001$) (Figure 8(c)). ROC curve suggested that circFCHO2 in serum exosomes was a sensitive and effective diagnostic marker for GC patients (Figure 8(d)).

Discussion

circRNAs are stable and conservative due to its closed-loop structure. The main function of circRNAs is to be sponges of miRNAs in the cytoplasm via competitively binding to response elements of miRNAs [23]. Interestingly, miRNAs can further regulate the expression of its downstream coding genes via binding to the 3′-untranslated region (3′-UTR) of mRNAs [24]. Therefore, circRNAs can indirectly regulate the expression of coding genes via sponging miRNAs, and finally participate in the regulation of biological processes. circRNAs are crucial modulators in multiple pathological processes of human diseases, such as vascular diseases, neurological disorders, especially malignant tumors [25]. It is more superior as therapeutic target than linear transcripts due to its unique structural stability [26]. This study demonstrated that the aberrantly up-regulated circFCHO2 in GC patients was

correlation between miR-194-5p and circFCHO2 in tumor tissues of GC patients. (E) The expression of miR-194-5p in cell lines was detected by qRT-PCR. (F) The binding site of circFCHO2 and miR-194-5p. (G) Dual-luciferase reporter gene assay. (H) RIP experiment was employed to detect the binding of circFCHO2 and miR-194-5p. (I) miR-194-5p expression in the transfected GC cells was determined by qRT-PCR. *** $P < 0.001$.

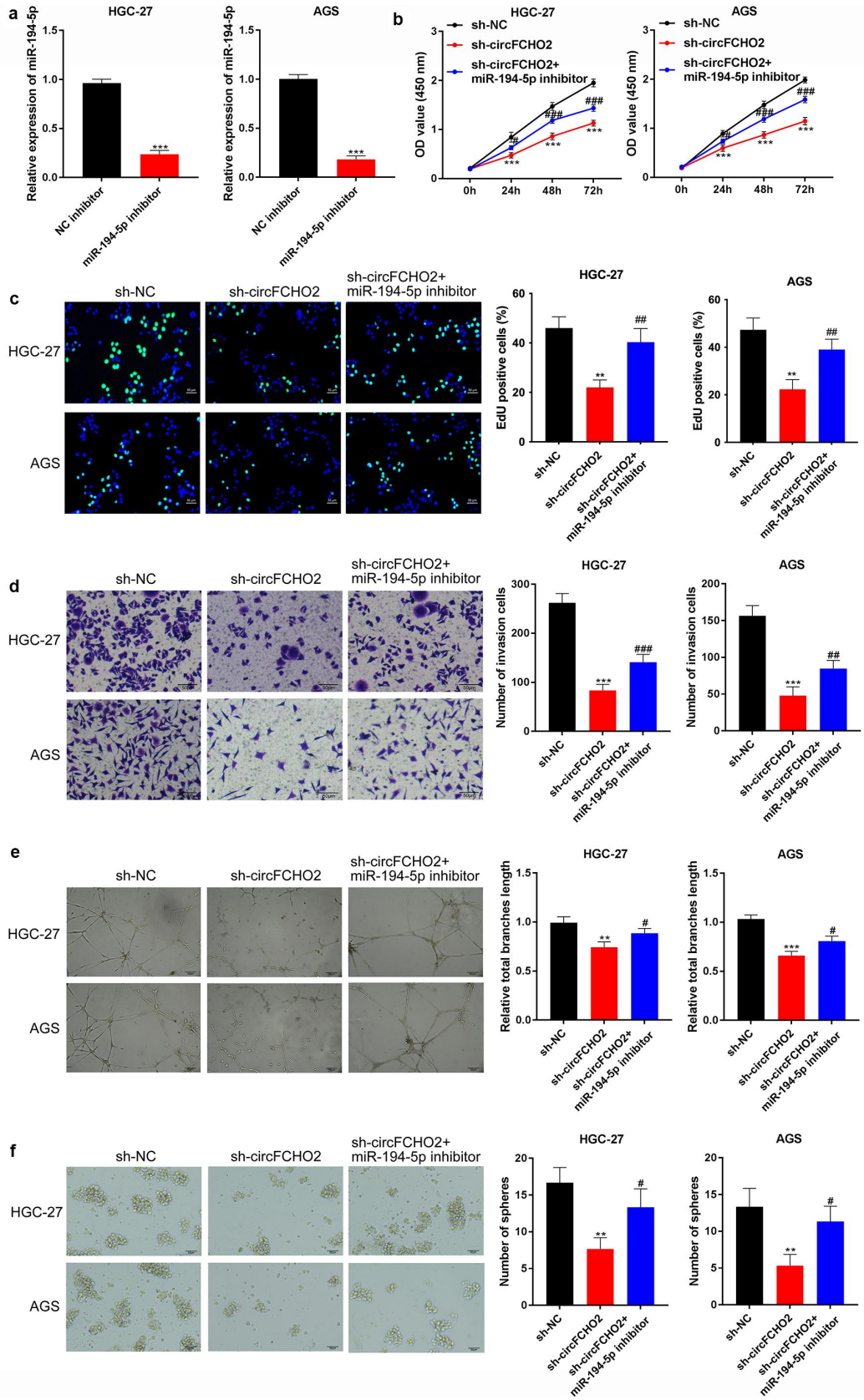

Figure 4. miR-194-5p knockdown partially reversed the inhibition of circFCHO2 silencing on the malignant phenotype of GC cells. (A) Transfection efficiency of GC cells was explored by qRT-PCR. *** $P < 0.001$. (B) The proliferation ability of GC cells was researched by CCK-8 assay. (C) EDU staining was carried out to evaluate the proliferation ability of GC cells. (D) The invasion ability of GC cells was detected by transwell experiment. (E) The angiogenesis ability of GC cells was evaluated by tube formation experiment. (F) The cancer stem cell characteristics of GC cells was assessed by spheroidization experiment. ** $P < 0.01$ or *** $P < 0.001$ vs. sh-NC group. # $P < 0.05$ or ## $P < 0.01$ or ### $P < 0.001$ vs. sh-circFCHO2 group.

associated with unfavorable clinical outcome. circFCHO2 was mainly expressed in the cytoplasm of GC cells. circFCHO2 silencing not only weakened the in vitro malignant phenotype of GC cells, such as proliferation, invasion, angiogenesis and cancer stem cell characteristics, but also attenuated the in vivo growth and lung metastasis of GC. Regarding the mechanism, circFCHO2 might be conductive to GC progression by activating the JAK1/STAT3 signaling pathway via sponging miR-194-5p. At present, the exact function of circFCHO2 on the progression of GC as well as other solid tumors has never been revealed. This study initially proved that circFCHO2 played the cancer-promoting role in GC. It could be used as an effective target for the treatment of GC.

miRNAs are a class of small non-coding RNA molecules with 21–22 nucleotides in length, which can regulate the expression of more than 60% of all human protein-coding genes at the post-transcriptional level [27]. It possesses crucial role in regulating multiple cellular biological processes, especially proliferation, apoptosis and metastasis involved in tumorigenesis and progression [28]. As a member of the miRNAs family, miR-194-5p has been discovered to be abnormally low expressed in GC patients. miR-194-5p expression could be directly reduced by long non-coding RNA (lncRNA) SOX2OT. Functionally, the up-regulation of miR-194-5p could abrogate the promotion of SOX2OT on the proliferation and invasion of GC cells [29]. Similarly, Ding et al. [30] declared that lncRNA TP73-AS1 could accelerate the progression of GC through sponging miR-194-5p. Additionally, miR-194-5p knockdown can facilitate the epithelial mesenchymal transition (EMT) of GC cells [31]. Consistently, the results of this study illustrated that miR-194-5p was lower expressed in GC patients and cells. As a target of circFCHO2, miR-194-5p expression was directly suppressed by circFCHO2. More importantly, miR-194-5p knockdown partially counteracted the inhibition of circFCHO2 silencing on the proliferation, invasion, angiogenesis and cancer stem cell characteristics of GC cells.

In this study, JAK1 was detected to be over-expressed in GC patients and cells, and it was researched to be a target of miR-194-5p. circFCHO2 knockdown reduced the expression of JAK1 and p-STAT3. Interestingly, miR-194-5p inhibitor abrogated this effect. Moreover, JAK1 overexpression partially reversed the inhibition of miR-194-5p on the malignant phenotype of GC cells. However, the expression of STAT3 was not obviously changed by circFCHO2, miR-194-5p and JAK1. All of these data indicated that circFCHO2 could enhance the progression of GC by activating the JAK1/STAT3 signaling pathway via sponging miR-194-5p. The JAK/STAT signaling pathway exerts an important function in regulating the progression of tumors [32]. It can accelerate the oncogenic phenotypes, such as metastasis, proliferation, apoptosis inhibition, angiogenesis, cancer stem cell characteristics and immune evasion [33,34]. The overexpressed JAK can promote the phosphorylation of STAT proteins. After being transferred to the nucleus, the activated STAT proteins can accelerate the carcinogenesis via activating its downstream oncogenes [35,36]. JAK1 is a main member of the JAK family, which can result in the persistent activation of oncogene STAT3 [33]. Previous studies have researched that the activated JAK1/STAT3 signaling pathway could facilitate the malignant development of GC [19,37]. This article explored for the first time that circFCHO2 could facilitate the progression of GC by activating the JAK1/STAT3 signaling pathway via sponging miR-194-5p.

Additionally, serum exosomes from GC patients and healthy participants were isolated to detect circFCHO2 expression. The results revealed that circFCHO2 was abnormally up-modulated in the serum exosomes of GC patients. Exosomes are extracellular vesicles with a diameter of 40–100 nm, which can be secreted by multiple types of cells. Exosomes carry abundant RNAs and proteins, and these vesicle contents are capable of mediating intercellular communication by being released into target cells [38]. Some circRNAs have been identified in the serum exosomes of GC patients, and these circRNAs levels in the serum exosomes are highly specific and sensitive markers for early GC screening and prognosis [39,40]. In this work, ROC curve illustrated that circFCHO2 level in the serum exosomes of GC patients had higher specificity and sensitivity to

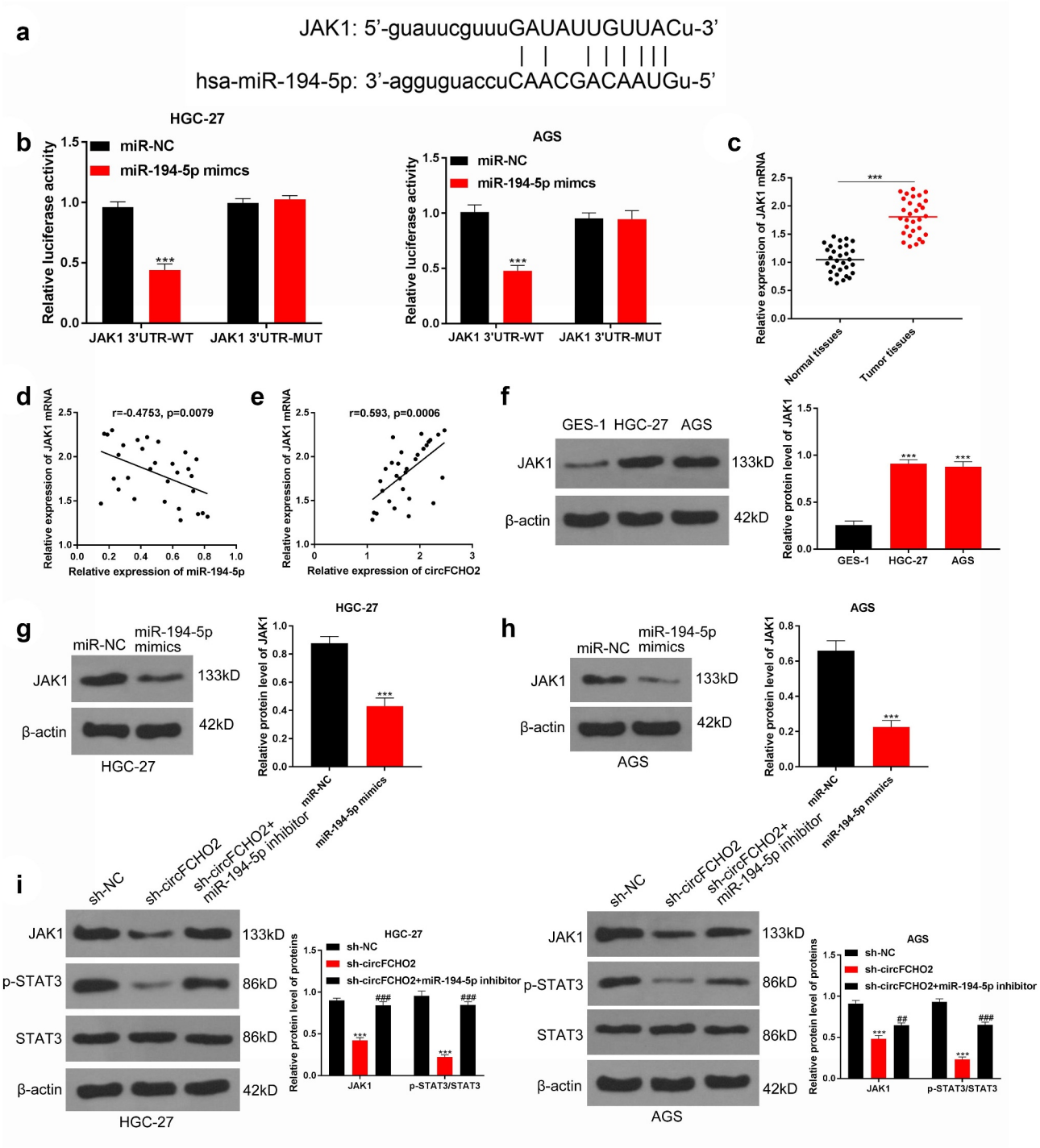

Figure 5. circFCHO2 promoted the activity of the JAK1/STAT3 pathway by sponging miR-194-5p.

(A) JAK1 contained mutual binding site of circFCHO2. (B) Dual-luciferase reporter gene assay. *** $P < 0.001$. (C) JAK1 expression in the 30 GC patients was explored by qRT-PCR. *** $P < 0.001$. (D and E) Pearson's correlation analysis was carried out to research the correlation between JAK1 and miR-194-5p or circFCHO2. (F) The expression of JAK1 protein in cells was detected by Western blot. *** $P < 0.001$. (G and H) The expression of JAK1 protein in the transfected GC cells was researched through Western blot. *** $P < 0.001$. (I) The expression of JAK1 and p-STAT3/STAT3 proteins in the transfected GC cells was investigated by Western blot. *** $P < 0.001$ vs. sh-NC group. ## $P < 0.01$ or ### $P < 0.001$ vs. sh-circFCHO2 group.

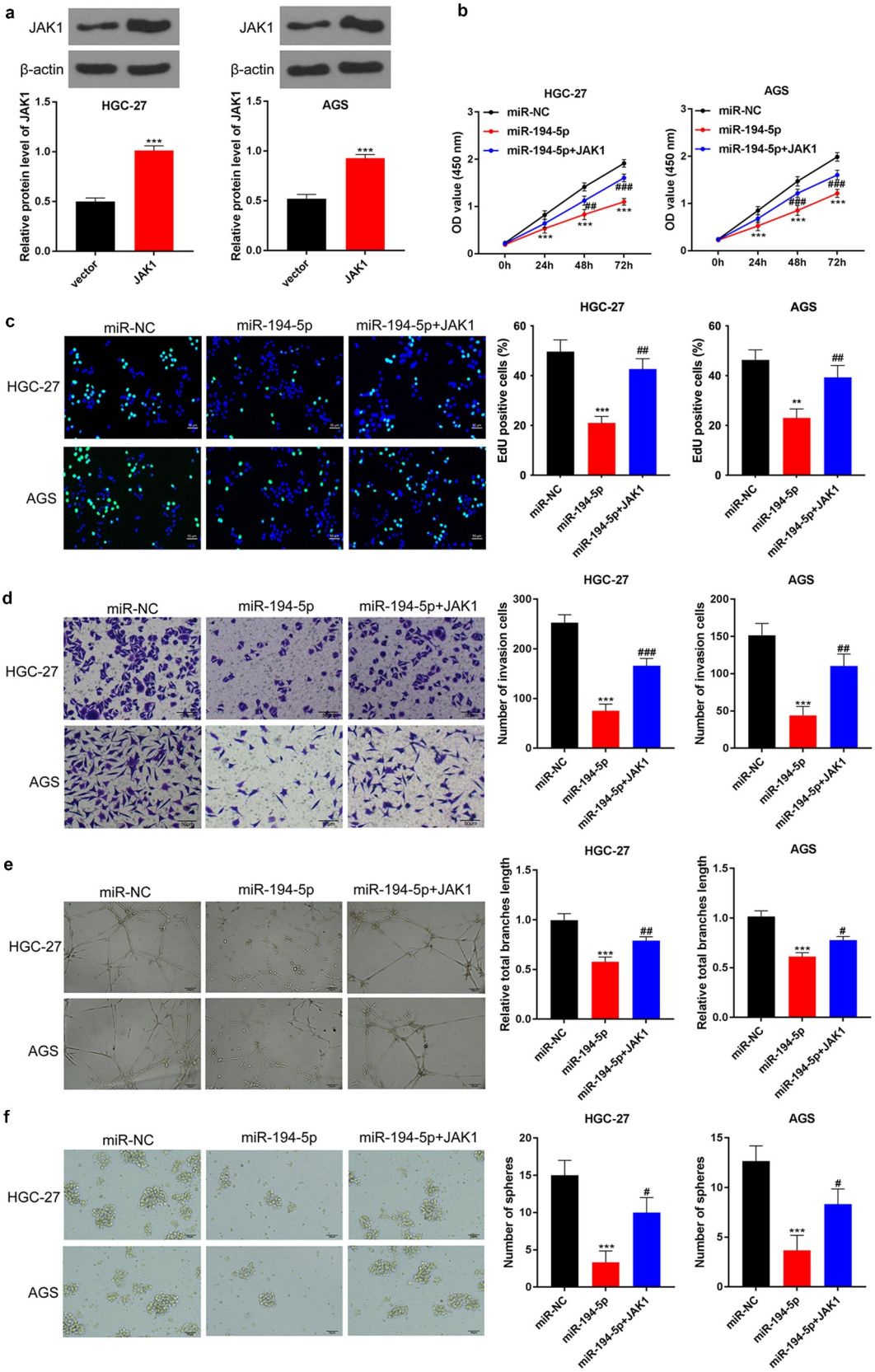

Figure 6. JAK1 overexpression partially reversed the inhibition of miR-194-5p on the malignant phenotype of GC cells.

(A) The expression of JAK1 protein in the transfected GC cells was monitored by Western blot. *** $P < 0.001$. (B) The proliferation ability of GC cells was assessed by CCK-8 assay. (C) EDU staining was used to reflect the proliferation ability of GC cells. (D) The invasion ability of GC cells was detected by transwell experiment. (E) The angiogenesis ability of GC cells was investigated by tube formation experiment. (F) The cancer stem cell characteristics of GC cells was evaluated by spheroidization experiment. *** $P < 0.001$ vs. miR-NC group. # $P < 0.05$ or ## $P < 0.01$ or ### $P < 0.001$ vs. miR-194-5p group.

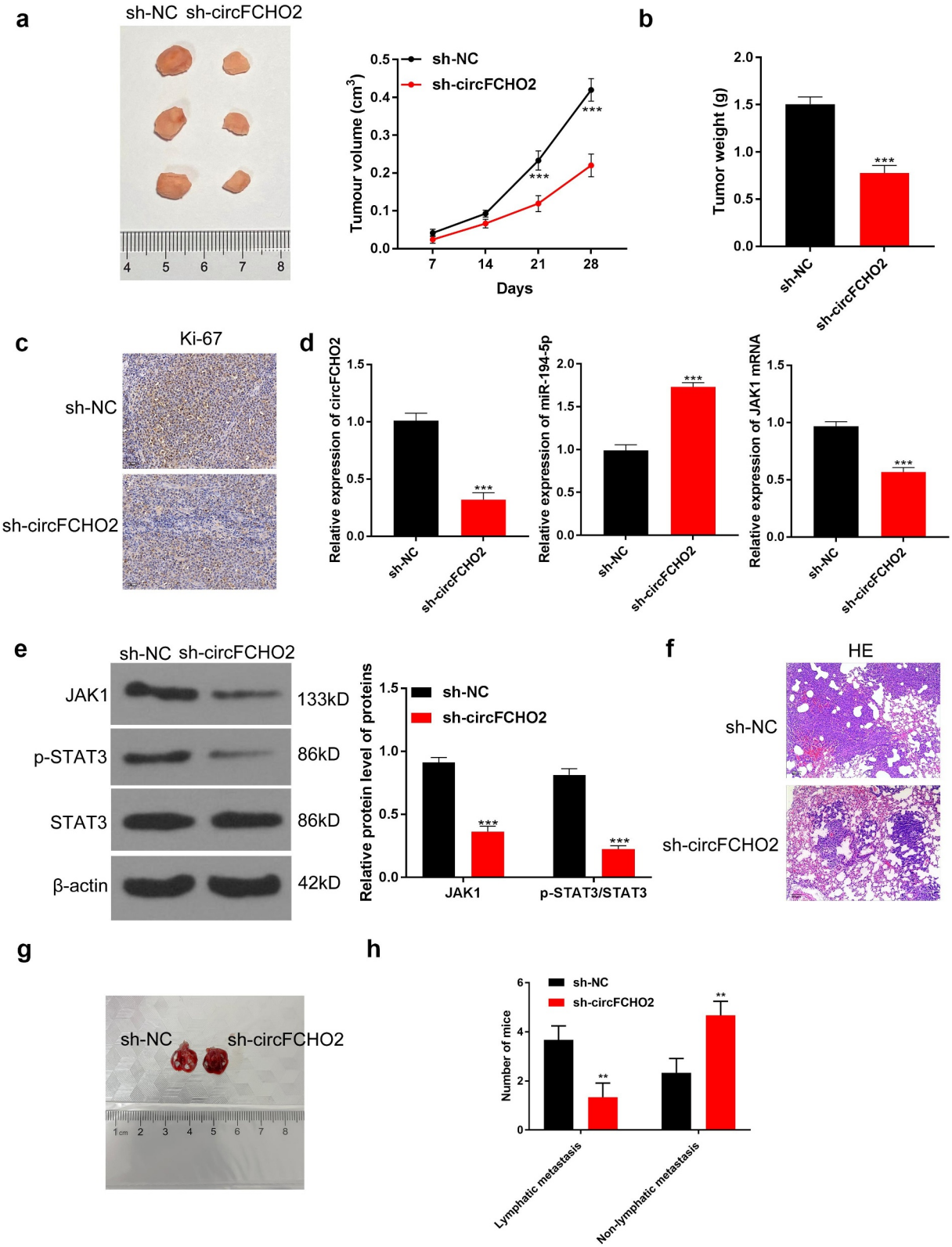

Figure 7. circFCHO2 silencing weakened the in vivo growth and lung metastasis of GC.

(A and B) The volume and weight of xenograft tumor in nude mice was monitored. (C) IHC was applied to monitor the expression of Ki67 protein in xenograft tumor. (D) The expression of circFCHO2, miR-194-5p and JAK1 mRNA in xenograft tumor was explored by qRT-PCR. (E) Western blot was used to research the expression of JAK1, p-STAT3 and STAT3 proteins in xenograft tumor. (F) HE staining was applied to detect the nodules in lung tissues of mice. (G) The original images of lung nodules. (H) The number of mice with or without lymphatic metastasis in each group. *** $P < 0.001$.

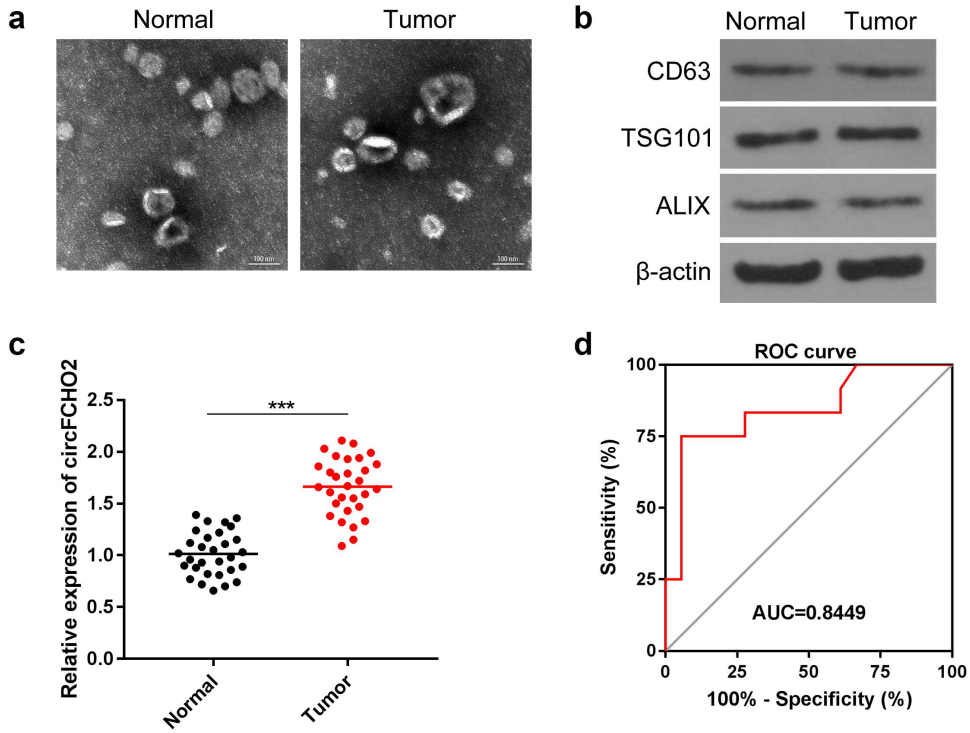

Figure 8. circFCHO2 in serum exosomes was a sensitive and effective biomarker for the diagnosis of GC.

(A) Serum exosomes of GC patients and healthy participants were isolated. TEM was used for the observation of serum exosomes. (B) Markers of exosomes were researched by Western blot. (C) circFCHO2 expression in the serum exosomes of GC patients and healthy participants was researched by using qRT-PCR. (D) ROC curve was used to analyze the potential of circFCHO2 as a diagnostic marker for GC patients. *** $P < 0.001$.

be a diagnostic indicator of GC. Thus, circFCHO2 level in the serum exosomes could be used as a novel diagnostic marker in GC clinically.

Of course, this study has limitations. In this study, in vivo lung metastases of GC were investigated. Thus, it should be better to use a metastatic GC cell line to perform the experiments relevant to the metastasis and invasion. Moreover, survival analysis of mice with lung metastases and metastatic site analysis in mice should be performed. However, due to the limitations of laboratory conditions, this issue cannot currently be performed. These interesting issues will be the focus in our future research.

In summary, this article firstly reported the exact function of circFCHO2 on GC progression. circFCHO2 was overexpressed in GC patients and cells, associating with poor clinical outcome of patients. circFCHO2 silencing could attenuate the in vitro malignant phenotype of GC cells, including proliferation, invasion, angiogenesis and cancer stem cell characteristics. Furthermore, circFCHO2 silencing weakened the in vivo growth and lung metastasis of GC. In terms of mechanism, circFCHO2 might enhance the progression of GC by activating the JAK1/STAT3 signaling pathway via sponging miR-194-5p. Moreover, circFCHO2 was abnormally up-modulated in the serum exosomes of GC patients, which was specific and sensitive to be a diagnostic indicator of GC. Thus, circFCHO2 was identified as an oncogene in GC, which was anticipated to be an effective target for GC. Moreover, circFCHO2 level in the serum exosomes could be used as a promising diagnostic marker in GC clinically. This study provided a novel perspective for the target treatment and diagnosis of GC.

Disclosure statement

No potential conflict of interest was reported by the author (s).

Data availability statement

All the data used to support the findings of this study are included within the article.

Declarations and ethics statements

Ethical approval

This work had been approved by the ethics committee in line with the Declaration of Helsinki.

Informed consent from participants

The written informed consent had been voluntarily signed by all patients.

Funding

The author(s) reported that there is no funding associated with the work featured in this article.

References

[1] Waldum H, Fossmark R. Gastritis, Gastric Polyps and Gastric. Cancer. 2021;22(12):6548.

[2] Kang MY, Jung J, Koo J-W, et al. Increased risk of gastric cancer in workers with occupational dust exposure. Korean J Intern Med. 2021;36(Suppl 1):S18–s26.

[3] Wang B, Zhang Y, Qing T, et al. Comprehensive analysis of metastatic gastric cancer tumour cells using single-cell RNA-seq. Sci Rep. 2021;11(1):1141.

[4] Shao T, Pan YH, Xiong XD. Circular RNA: an important player with multiple facets to regulate its parental gene expression. Mol Ther Nucleic Acids. 2021;23:369–376.

[5] Li XW, Yang WH, Xu J. Circular RNA in gastric cancer. Chin Med J (Engl). 2020;133(15):1868–1877.

[6] Wang H, Sun G, Xu P, et al. Circular RNA TMEM87A promotes cell proliferation and metastasis of gastric cancer by elevating ULK1 via sponging miR-142-5p. J Gastroenterol. 2021;56(2):125–138.

[7] Bu X, Chen Z, Zhang A, et al. Circular RNA circAFF2 accelerates gastric cancer development by activating miR-6894-5p and regulating ANTXR 1 expression. Clin Res Hepatol Gastroenterol. 2021;45(3):101671.

[8] Fan D, Wang C, Wang D, et al. Circular RNA circ_0000039 enhances gastric cancer progression through miR-1292-5p/DEK axis. Cancer Biomark. 2021;30(2):167–177.

[9] Xu Q, Liao B, Hu S, et al. Circular RNA 0081146 facilitates the progression of gastric cancer by sponging miR-144 and up-regulating HMGB1. Biotechnology Letters. 2021;43(4):767–779.

[10] Liang M, Yao W, Shi B. Circular RNA hsa_circ_0110389 promotes gastric cancer progression through upregulating SORT1 via sponging miR-127-5p and miR-136-5p. Cell Death & Disease. 2021;12(7):639.

[11] Wang Y, Wang H, Zheng R, et al. Circular RNA ITCH suppresses metastasis of gastric cancer via regulating miR-199a-5p/Klotho axis. Cell Cycle. 2021;20(5–6):522–536.

[12] Guo X, Qin M, Hong H, et al. Circular RNA hsa_circ_0072309 inhibits the proliferation, invasion and migration of gastric cancer cells via inhibition of PI3K/AKT signaling by activating PPARγ/PTEN signaling. Mol Med Rep. 2021;23(5). DOI:10.3892/mmr.2021.11988.

[13] Li H, Shan C, Wang J, et al. CircRNA Hsa_circ_0001017 inhibited gastric cancer progression via acting as a sponge of miR-197. Digestive Diseases and Sciences. 2021;66(7):2261–2271.

[14] Wang H, Wang N, Zheng X, et al. Circular RNA hsa_circ_0009172 suppresses gastric cancer by regulation of microRNA-485-3p-mediated NTRK3. Cancer Gene Therapy. 2021;28(12):1312–1324.

[15] Papaioannou D, Volinia S, Nicolet D, et al. Clinical and functional significance of circular RNAs in cytogenetically normal AML. Blood Adv. 2020;4(2):239–251.

[16] Jie M, Wu Y, Gao M, et al. CircMRPS35 suppresses gastric cancer progression via recruiting KAT7 to govern histone modification. Mol Cancer. 2020;19(1):56.

[17] Ding Z, Kloss JM, Tuncali S, et al. TROY signals through JAK1-STAT3 to promote glioblastoma cell migration and resistance. Neoplasia. 2020;22(9):352–364.

[18] Zhou Y, Xu XM, Feng Y. MiR-769-5p inhibits cancer progression in oral squamous cell carcinoma by directly targeting JAK1/STAT3 pathway. Neoplasma. 2020;67(3):528–536.

[19] Chen W, Wu G, Zhu Y, et al. HOXA10 deteriorates gastric cancer through activating JAK1/STAT3 signaling pathway. Cancer Manag Res. 2019;11:6625–6635.

[20] Li Z, Chen J. miR-583 inhibits the proliferation and invasion of prostate cancer cells by targeting JAK1. Mol Med Rep. 2021;23(3):247.

[21] Mao J, Hu X, Pang P, et al. miR-30e acts as a tumor suppressor in hepatocellular carcinoma partly via JAK1/STAT3 pathway. Oncol Rep. 2017;38(1):393–401.

[22] Liu X, Shen S, Zhu L, et al. SRSF10 inhibits biogenesis of circ-ATXN1 to regulate glioma angiogenesis via miR-526b-3p/MMP2 pathway. J Exp Clin Cancer Res. 2020;39(1):121.

[23] Luo Z, Rong Z, Zhang J, et al. Circular RNA circCCDC9 acts as a miR-6792-3p sponge to suppress the progression of gastric cancer through regulating CAV1 expression. Mol Cancer. 2020;19(1):86.

[24] Sun G, Li Z, He Z, et al. Circular RNA MCTP2 inhibits cisplatin resistance in gastric cancer by miR-99a-5p-mediated induction of MTMR3 expression. J Exp Clin Cancer Res. 2020;39(1):246.

[25] Yan F, Fan B, Wang J. Circ_0008305-mediated miR-660/BAG5 axis contributes to hepatocellular carcinoma tumorigenesis. Cancer Medicine. 2021;10(3):833–842.

[26] Chen YW, Du Q-R, He Y-J, et al. Circ_0044516 regulates miR-136/MAT2A pathway to facilitate lung cancer

development. Journal of Immunology Research. 2021;2021:5510869.
[27] Kurata JS, Lin RJ. MicroRNA-focused CRISPR-Cas9 library screen reveals fitness-associated miRNAs. RNA . 2018;24(7):966–981.
[28] Patil N, Allgayer H, Leupold JH. MicroRNAs in the Tumor Microenvironment. Adv Exp Med Biol. 2020;1277:1–31.
[29] Qu F, Cao P. Long noncoding RNA SOX2OT contributes to gastric cancer progression by sponging miR-194-5p from AKT2. Exp Cell Res. 2018;369(2):187–196.
[30] Ding Z, Lan H, Xu R, et al. LncRNA TP73-AS1 accelerates tumor progression in gastric cancer through regulating miR-194-5p/SDAD1 axis. Pathol Res Pract. 2018;214 (12):1993–1999.
[31] Wei R, Ding C, Rodrìguez RA, et al. The SOX2OT/miR-194-5p axis regulates cell proliferation and mobility of gastric cancer through suppressing epithelial-mesenchymal transition. Oncol Lett. 2018;16(5):6361–6368.
[32] Huang Y, Cen L-P, Choy KW, et al. JAK/STAT pathway mediates retinal ganglion cell survival after acute ocular hypertension but not under normal conditions. Exp Eye Res. 2007;85(5):684–695.
[33] Chen B, Lai J, Dai D, et al. JAK1 as a prognostic marker and its correlation with immune infiltrates in breast cancer. Aging (Albany NY). 2019;11(23):11124–11135.
[34] Toh TB, Lim JJ, Hooi L, et al. Targeting Jak/Stat pathway as a therapeutic strategy against SP/CD44+ tumorigenic cells in Akt/β-catenin-driven hepatocellular carcinoma. J Hepatol. 2020;72(1):104–118.
[35] Spano JP, Milano G, Rixe C, et al. JAK/STAT signalling pathway in colorectal cancer: a new biological target with therapeutic implications. Eur J Cancer. 2006;42(16):2668–2670.
[36] Mullen M, Gonzalez-Perez RR. Leptin-induced JAK/STAT signaling and cancer growth. Vaccines (Basel). 2016;4(3):26.
[37] Su C, Wang W, Wang C. IGF-1-induced MMP-11 expression promotes the proliferation and invasion of gastric cancer cells through the JAK1/STAT3 signaling pathway. Oncol Lett. 2018;15(5):7000–7006.
[38] Zang R, Qiu X, Song Y, et al. Exosomes mediated transfer of Circ_0000337 contributes to cisplatin (CDDP) resistance of esophageal cancer by regulating JAK2 via miR-377-3p. Front Cell Dev Biol. 2021;9:673237.
[39] Xie M, Yu T, Jing X, et al. Exosomal circSHKBP1 promotes gastric cancer progression via regulating the miR-582-3p/HUR/VEGF axis and suppressing HSP90 degradation. Molecular Cancer. 2020;19(1):112.
[40] Shao Y, Tao X, Lu R, et al. Hsa_circ_0065149 is an indicator for early gastric cancer screening and prognosis prediction. Pathology Oncology Research: POR. 2020;26(3):1475–1482.